Proceedings of the Combustion Institute, Volume 28, 2000/pp. 2029–2037

EXTINCTION AND AUTOIGNITION OF *n*-HEPTANE IN COUNTERFLOW CONFIGURATION

R. SEISER,[1] H. PITSCH,[1] K. SESHADRI,[1] W. J. PITZ[2] AND H. J. CURRAN[2]

[1]*Department of Mechanical and Aerospace Engineering*
University of California at San Diego
La Jolla, California 92093-0417, USA
[2]*Lawrence Livermore National Laboratory*
P. O. Box 808
Livermore, California 94551, USA

A study was performed to elucidate the mechanisms of extinction and autoignition of *n*-heptane in strained laminar flows under non-premixed conditions. A previously developed detailed mechanism made up of 2540 reversible elementary reactions among 556 species was the starting point for the study. The detailed mechanism was previously used to calculate ignition delay times in homogeneous reactors, and concentration histories of a number of species in plug-flow and jet-stirred reactors. An intermediate mechanism made up of 1282 reversible elementary reactions among 282 species and a short mechanism made up of 770 reversible elementary reactions among 159 species were assembled from this detailed mechanism. Ignition delay times in an isochoric homogeneous reactor calculated using the intermediate and the short mechanism were found to agree well with those calculated using the detailed mechanism. The intermediate and the short mechanism were used to calculate extinction and autoignition of *n*-heptane in strained laminar flows. Steady laminar flow of two counterflowing streams toward a stagnation plane was considered. One stream, made up of prevaporized *n*-heptane and nitrogen, was injected from the fuel boundary, and the other stream, made up of air and nitrogen, was injected from the oxidizer boundary. Critical conditions of extinction and autoignition given by the strain rate, temperature, and concentrations of the reactants at the boundaries were calculated. The results were found to agree well with experiments. Sensitivity analysis was carried out to evaluate the influence of various elementary reactions on autoignition. At all values of the strain rate investigated here, high-temperature chemical processes were found to control autoignition. In general, the influence of low-temperature chemistry was found to increase with decreasing strain. A key finding of the present study is that strain has more influence on low-temperature chemistry than the temperature of the reactants.

Introduction

Chemical-kinetic mechanisms that describe oxidation of *n*-heptane (*n*-C_7H_{16}) have been developed by numerous investigators [1–13]. *n*-Heptane is a primary reference fuel for octane rating in internal combustion engines. It has a cetane number of approximately 56, which is similar to the cetane number of conventional diesel. Recently, a comprehensive chemical-kinetic mechanism was developed to describe combustion of *n*-heptane [10]. Numerical calculations were performed using this mechanism, and the results were compared with experimental data obtained in flow reactors, shock tubes, and rapid compression machines. Here, chemical-kinetic mechanisms are assembled from this comprehensive mechanism and are used to describe extinction and autoignition of *n*-heptane in non-premixed systems. The results are compared with experiments conducted in the counterflow configuration [12–14].

The present study was motivated by a need to develop chemical-kinetic mechanisms that can be used in computational fluid dynamic codes to model combustion and transport processes taking place in diesel engines. Combustion processes in diesel engines closely resemble non-premixed systems. Previous experimental studies on autoignition were focused on measuring ignition delay times in shock tubes [15] and rapid compression machines [16–18]. These studies were conducted on premixed systems and revealed various aspects of *n*-heptane autoignition and combustion. The present study addresses extinction and autoignition of *n*-heptane in counterflow non-premixed systems where transport processes play an important role. Computational resources required for calculating aspects of autoignition in a one-dimensional counterflow configuration are significantly larger than those required in a homogeneous system. Large reaction mechanisms, such as those for *n*-heptane, need to be reduced to make the numerical problem tractable in one-dimensional configurations.

Lindstedt and Maurice [5] have developed a detailed chemical-kinetic mechanism for describing

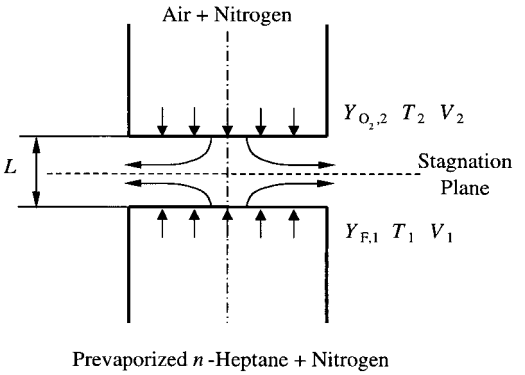

FIG. 1. Schematic illustration of the counterflow configuration.

the oxidation of *n*-heptane. This mechanism has been tested by comparing numerical results with experimental data obtained in stirred reactors, counterflow non-premixed flames, and premixed flames. This was one of the first attempts to develop a chemical-kinetic mechanism for *n*-heptane which can be applied to flames where transport processes are important, and to stirred reactors. This mechanism, however, did not address ignition and extinction of non-premixed flames. Seiser et al. [12] calculated the structure and critical conditions of extinction of non-premixed *n*-heptane flames and compared the results with experimental measurements. This study employed a chemical-kinetic mechanism which had been previously simplified by introducing ad hoc approximations [8]. At given concentrations of the reactants, the calculated strain rate at extinction was found to be higher than that measured [12]. Here, critical conditions of extinction are calculated using mechanisms that were deduced from the comprehensive mechanism of Curran et al. [10], and the results are compared with experimental data shown in Ref. [12]. Experimental data for the critical conditions of autoignition of *n*-heptane in the counterflow configuration are given in Refs. [13,14]. Using these experimental data, overall chemical-kinetic rate parameters that characterize the rate of one-step overall reaction between fuel and oxygen were obtained [14]. Here, critical conditions of autoignition are calculated using mechanisms that were deduced from the comprehensive mechanism [10], and the results are compared with experimental data shown in Refs. [13,14].

Description of Experimental and Numerical Studies in the Counterflow Configuration

Steady, axisymmetric, laminar flow of two counterflowing streams toward a stagnation plane was considered. Fig. 1 shows a schematic illustration of the counterflow configuration employed in previous experimental studies [12–14] and in the present numerical study. In this configuration, a fuel stream made up of prevaporized *n*-heptane and nitrogen is injected from one duct, called the fuel duct, and an oxidizer stream made up of air and nitrogen is injected from the other duct, called the oxidizer duct. These jets flow into the mixing layer between the two ducts. The exit of the fuel duct is the fuel boundary, and the exit of the oxidizer duct is the oxidizer boundary. The mass fraction of fuel, the temperature, and the component of the flow velocity normal to the stagnation plane at the fuel boundary are represented by $Y_{F,1}$, T_1, and V_1, respectively. The mass fraction of oxygen, the temperature, and the component of the flow velocity normal to the stagnation plane at the oxidizer boundary are represented by $Y_{O_2,2}$, T_2, and V_2, respectively. The tangential components of the flow velocities at the boundaries are presumed to be equal to zero. The distance between the fuel boundary and the oxidizer boundary is represented by L.

In the experiments and numerical calculations, the momenta of the counterflowing reactant streams $\rho_i V_i^2$, $i = 1, 2$ at the boundaries are kept equal to each other. Here, ρ_1 and ρ_2 represent the density of the mixture at the fuel boundary and the oxidizer boundary, respectively. This condition ensures that the stagnation plane formed by the two streams is approximately in the middle of the region between the two boundaries. The value of the strain rate, defined as the normal gradient of the normal component of the flow velocity, changes from the fuel boundary to the oxidizer boundary [19]. The characteristic strain rate on the oxidizer side of the stagnation plane, a_2, is presumed to be given by [19]

$$a_2 = \frac{2|V_2|}{L}\left(1 + \frac{|V_1|\sqrt{\rho_1}}{|V_2|\sqrt{\rho_2}}\right) \qquad (1)$$

Equation 1 is obtained from an asymptotic theory in which the Reynolds numbers of the laminar flow at the boundaries are presumed to be large [19]. Critical conditions of extinction are presumed to be given by the strain rate, $a_{2,e}$, the temperatures, and the mass fraction of fuel and oxygen at the boundaries. Critical conditions of autoignition are presumed to be given by the strain rate, $a_{2,I}$, the temperature of the oxidizer stream, $T_{2,I}$, the temperature of the fuel stream, and the mass fraction of fuel and oxygen at the boundaries. The experiments were conducted at a pressure of 1.013 bar.

Experimental Procedure

A detailed description of the burners has been given elsewhere [12–14]. The flow rates of gases were measured by computer-regulated mass flow controllers. The velocities of the reactants at the

boundaries were presumed to be equal to the ratio of their volumetric flowrates to the cross-sectional area of the ducts. The temperature of the fuel stream and the temperature of the oxidizer stream at the boundaries were measured using thermocouples. A brief description of the experimental procedure is given here.

Critical Conditions of Extinction

Extinction experiments were previously carried out allowing only small changes in the flame position in the reactive flow field [12]. It is convenient to express the flame position in terms of a conserved scalar quantity ξ, called the mixture fraction. The mixture fraction is so defined that $\xi = 1.0$ in the fuel stream and $\xi = 0$ in the oxidizer stream [20]. The location of the flamesheet, ξ_{st}, where the flux of the fuel and the flux of oxygen are in stoichiometric proportion, is given by $\xi_{st} = [1 + 11Y_{F,1}W_{O_2}/(Y_{O_2,2}W_F)]^{-1}$, where W_F and W_{O_2} represent the molecular weights of fuel and oxygen, respectively. Extinction experiments were performed keeping ξ_{st} constant at 0.1. The temperature of the fuel stream was $T_1 = 345$ K, and the temperature of the oxidizer stream was $T_2 = 298$ K. The distance between the fuel boundary and the oxidizer boundary was $L = 10$ mm. At some selected value of $Y_{O_2,2}$, the flame was stabilized at $a_2 < a_{2,e}$. The strain rate was increased by increasing V_1 and V_2 until extinction was observed. Experimental results are shown later.

Critical Conditions of Autoignition

Previous autoignition experiments were conducted with the mass fraction of prevaporized fuel, $Y_{F,1}$, maintained at 0.387 [13,14]. The temperature at the fuel boundary, T_1, was 378 K. The oxidizer stream was air with a mass fraction of oxygen $Y_{O_2,2} = 0.233$. The distance between the fuel boundary and the oxidizer boundary was $L = 12$ mm. At a given strain rate and oxidizer temperature, $T_2 < T_{2,I}$, the flow field was established. The temperature at the oxidizer boundary was gradually increased until autoignition took place. Experimental results are shown later.

Formulation of the Numerical Problem

The conservation equations of mass, momentum, and energy and the species balance equations used in the formulation of the numerical problem have been summarized elsewhere [8,21,22]. The species balance equations include thermal diffusion, and the energy conservation equation includes radiative heat loss from carbon dioxide and water vapor [22]. Buoyancy is neglected. Calculations are performed over a computational domain of 10 mm to obtain the critical conditions of extinction and over a computational domain of 12 mm to obtain the critical conditions of autoignition. At both ends of the computational domain, the mass fractions of the reactants and the normal components of the flow velocity are specified. The values of the tangential component of the flow velocity at both ends are set equal to zero (the so-called plug-flow boundary conditions). Critical conditions of extinction are calculated with $T_1 = 345$ K and $T_2 = 298$ K. Critical conditions of autoignition are calculated with $T_1 = 378$ K. The characteristic strain rate at the stagnation plane is calculated using equation 1.

The chemical-kinetic mechanism used to calculate the critical conditions of extinction and autoignition was deduced from the comprehensive mechanism of Curran et al. [10]. This mechanism, called the detailed mechanism, comprises 2540 reversible elementary reactions among 555 species. The rate constant, k, of any elementary reaction in this mechanism is given by $k = BT^n \exp[-E/(\mathcal{R}T)]$, where T is the temperature and $\mathcal{R}$ is the gas constant. The frequency factor, B, the temperature exponent, n, and the activation energy, E, are the rate parameters. This comprehensive mechanism was previously used to calculate ignition delay times in homogeneous reactors, and concentration histories of a number of species in plug-flow and jet-stirred reactors. The results were found to agree with experiments [10]. Improvements have been made to this mechanism [23]. Rate parameters for the forward rate constant of alkyl radical R addition to oxygen represented by the elementary reaction $R + O_2 = RO_2$ is now given by $B = 4.52 \times 10^{12}$ cm^3/(mol s), $n = 0$, and $E = 0$ for the primary, $B = 7.54 \times 10^{12}$ cm^3/(mol s), $n = 0$, and $E = 0$ for the secondary, and $B = 1.41 \times 10^{13}$ cm^3/(mol s), $n = 0$, and $E = 0$ for the tertiary alkyl radical. With the alkyl denoted by R′, rate parameters for the forward rate constant of the reaction $R'O_2 + R = R'O + RO$ are $B = 7.00 \times 10^{12}$ cm^3/(mol s), $n = 0$, and $E = -4184$ J/mol; for the reaction $RO_2 + HO_2 = RO_2H + O_2$, $B = 1.75 \times 10^{10}$ cm^3/(mol s), $n = 0$, and $E = -13702.58$ J/mol; and for the reaction $RO_2 + R'O_2 = O_2 + RO + R'O$, $B = 1.40 \times 10^{16}$ cm^3/(mol s), $n = -1.61$, and $E = 7782.23$ J/mol. Modifications in reaction rate rules were documented in Ref. [23]. Recent changes in the thermodynamic properties of peroxy radicals have been adopted [24,25].

The number of reactions and species in the detailed mechanism was reduced before it was used to calculate the critical conditions of extinction and autoignition in non-premixed systems. To reduce the mechanism, ignition delay times, τ_{ig}, in an isochoric homogeneous reactor configuration were calculated using the detailed mechanism. Ten conditions were selected, given by values of initial pressure equal to 1 bar and 13.5 bar and values of initial temperatures equal to 625 K, 740 K, 909 K, 1176 K, and 1667 K.

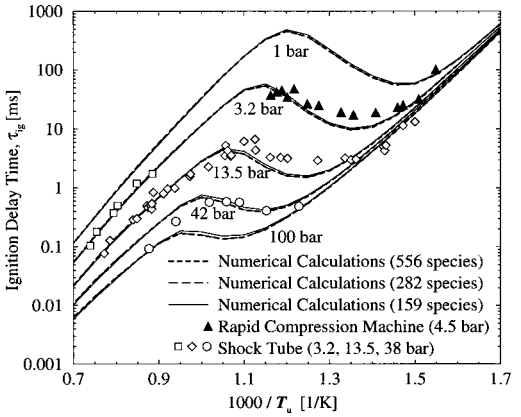

FIG. 2. Ignition delay time, τ_{ig}, in stoichiometric mixtures of *n*-heptane vapor and air as a function of the reciprocal of initial temperature, T_u, for various pressures. The short-dashed line represents τ_{ig} calculated using the detailed mechanism. The long-dashed line represents τ_{ig} calculated using the intermediate mechanism. The solid line represents τ_{ig} calculated using the short mechanism. The symbols represent experimental data obtained in shock tubes [15] and rapid compression machines [16].

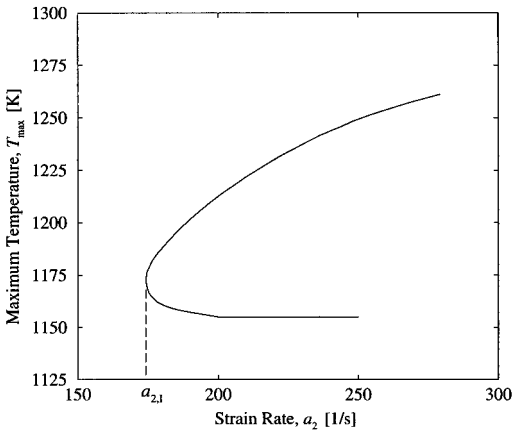

FIG. 3. The maximum temperature, T_{max}, as a function of the strain rate. Calculations are performed using the short mechanism for $T_2 = 1155$ K and $T_1 = 378$ K. The mass fraction of fuel in the fuel stream is $Y_{F,1} = 0.387$.

To test the influence of any given species on the ignition delay time, all elementary reactions in which this species appears were removed from the detailed mechanism, and the values of τ_{ig} were computed at the selected 10 conditions using the truncated detailed mechanism now made up of 555 species. The deviation of the ignition delay time calculated using this truncated mechanism from the ignition delay time calculated using the detailed mechanism was obtained. If the deviation at all conditions was less than 0.84%, this species was removed from the mechanism. Some species were retained in the mechanism even if the deviation was less than 0.84%, because their influence on critical conditions of extinction and autoignition was suspected to be greater than their influence on τ_{ig} in homogeneous reactors. Using this procedure, an intermediate mechanism made up of 1282 reversible reactions among 282 species was obtained. To reduce the mechanism further, the flame structure was calculated at one condition, and the structure of the reactive flow at two conditions close to autoignition. These calculations were made using the intermediate mechanism. For all species, the rates of production and consumption were computed. The results were used to determine the important chemical paths of fuel breakdown and oxidation. Species that appear only along paths where the rates of fuel breakdown and oxidation are small were deleted from the intermediate mechanism. This gave a short mechanism made up of 770 reversible elementary reactions among 159 species. The intermediate mechanism and the short mechanism are available in Ref. [26].

Figure 2 shows the ignition delay time, τ_{ig}, in stoichiometric mixtures of *n*-heptane-vapor and air as a function of the reciprocal of the initial temperature, T_u, for various values of pressure. All numerical results agree well with experimental data obtained in shock tubes [15] and in rapid compression machines [16]. Values of τ_{ig} calculated using the short mechanism agree well with those calculated using the detailed mechanism. The agreement between values of τ_{ig} calculated using the intermediate mechanism and the detailed mechanism is even better. A similar result was found when concentrations of key intermediate species including soot precursors were compared among the three mechanisms. The short and the intermediate mechanism were used to calculate the structure of the reactive flow-field in the counterflow configuration and critical conditions of extinction and autoignition.

Extinction and Autoignition

Figure 3 illustrates the procedure employed to deduce the strain rate at autoignition at a given value of T_2. The maximum temperature in the flow-field, T_{max}, is plotted in Fig. 5 as a function of the strain rate. This figure is the so-called C-shaped curve. For values of strain rate greater than $a_{2,I}$, two solutions obtained are shown in Fig. 3. The solution with the lower value of the maximum temperature is stable, while the solution with the higher value of the maximum temperature is unstable. The quantity $a_{2,I}$ represents the strain rate at autoignition. A similar procedure is employed to obtain the critical conditions of extinction.

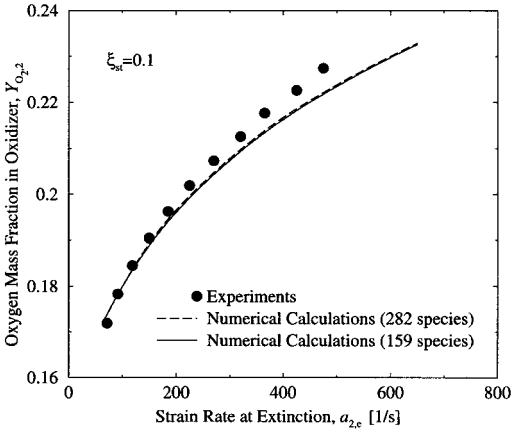

FIG. 4. Mass fraction of oxygen in the oxidizer stream at extinction, $Y_{O_2,2}$, as a function of the strain rate, $a_{2,e}$. The symbols represent measurements [12]. The solid line represents results of numerical calculations performed using the short chemical-kinetic mechanism. The dashed line represents results of numerical calculations performed using the intermediate chemical-kinetic mechanism.

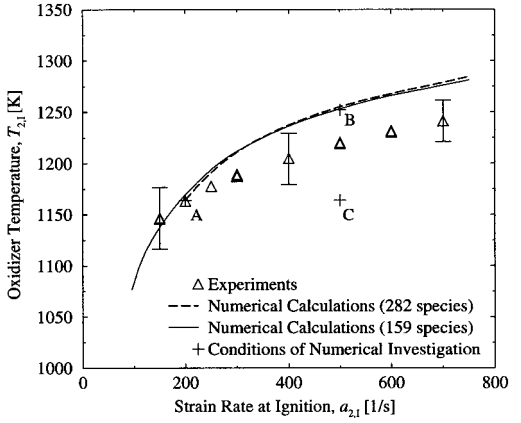

FIG. 5. Oxidizer temperature at autoignition, $T_{2,I}$, as a function of the strain rate, $a_{2,I}$. The triangles represent measurements [13,14]. The solid line represents results of numerical calculations performed using the short chemical-kinetic mechanism. The dashed line represents results of numerical calculations performed using the intermediate chemical-kinetic mechanism. The plus symbols indicate conditions used in numerical investigation.

Figure 4 shows the mass fraction of oxygen in the oxidizer stream at extinction, $Y_{O_2,2}$, as a function of the strain rate, $a_{2,e}$. The symbols represent measurements reproduced from Ref. [12]. Fig. 4 shows that the results of numerical calculations obtained using the short mechanism agree well with those calculated using the intermediate mechanism. Numerical results agree well with experimental data. The agreement between the experimental data and numerical results shown in Fig. 4 is significantly better than that shown in Ref. [12].

Figure 5 shows the oxidizer temperature at autoignition, $T_{2,I}$, as a function of the strain rate, $a_{2,I}$. The symbols represent measurements reproduced from Refs. [13,14]. Fig. 5 shows that the results of numerical calculations performed using the short mechanism agree well with those calculated using the intermediate mechanism. Numerical results agree well with experimental data at low values of the strain rate. At high values of the strain rate, the numerical results show autoignition to take place at higher values of $T_{2,I}$ in comparison to those measured. The plus symbols in Fig. 5 indicate the conditions used in numerical investigation described in the following section.

Influence of Strain on Autoignition

Analysis was carried out to investigate the role of strain on autoignition. Numerical calculations were performed at three conditions identified here as case A, case B, and case C. Case A refers to calculations at $a_2 = 200\ s^{-1}$ and $T_2 = 1164$ K, case B at $a_2 = 500\ s^{-1}$ and $T_2 = 1252$ K, and case C at $a_2 = 500\ s^{-1}$ and $T_2 = 1164$ K. Calculations were performed using the short mechanism for $Y_{F,1} = 0.387$, $T_1 = 378$ K, and $Y_{O_2,2} = 0.233$. At $a_2 = 200\ s^{-1}$, the calculated value of $T_{2,I} = 1165$ K, and at $a_2 = 500\ s^{-1}$, $T_{2,I} = 1253$ K. Thus, case A and case B are close to the critical conditions of autoignition.

Figure 6 shows the maximum value of the sensitivity coefficient for various elementary reactions given by $(k/Y_{OH})(\partial Y_{OH}/\partial k)_{max}$, where Y_{OH} is the mass fraction of OH. For all three cases, the top four reactions identified by the sensitivity analysis are the same, with the chain-branching reaction $H + O_2 = OH + O$ being the most important reaction. This chain-branching reaction plays a pivotal role in many applications where high-temperature chemical processes are dominant. Thus, the sensitivity analysis indicates that high-temperature chemical processes control autoignition in the non-premixed system investigated here.

It is of interest to focus on the differences among the three cases considered here. Fig. 6 shows the value of the sensitivity coefficient for the reactions $2\text{-}C_7H_{15}O_2 = 2\text{-}C_7H_{14}OOH\text{-}4$ and $3\text{-}C_7H_{15}O_2 = 3\text{-}C_7H_{14}OOH\text{-}5$ in case A to be much larger than those in cases B and C. They represent the second generic step in the reaction sequence that leads to chain branching under low-temperature conditions. The first generic step is heptyl radical addition to molecular oxygen to form $C_7H_{15}O_2$. This compound isomerizes (above) to $C_7H_{14}OOH$, followed by reaction

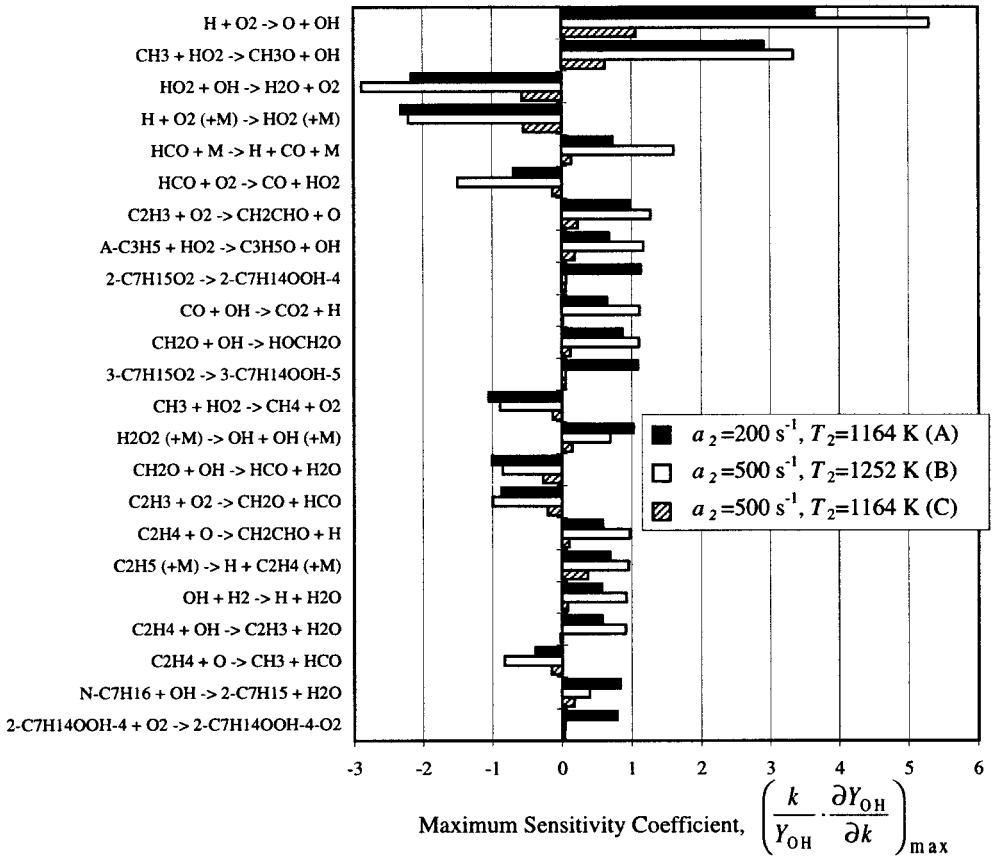

FIG. 6. Sensitivity coefficient for various elementary reactions. The sensitivities were calculated using the short mechanism for $Y_{F,1} = 0.387$, $T_1 = 378$ K, and $Y_{O_2,2} = 0.233$.

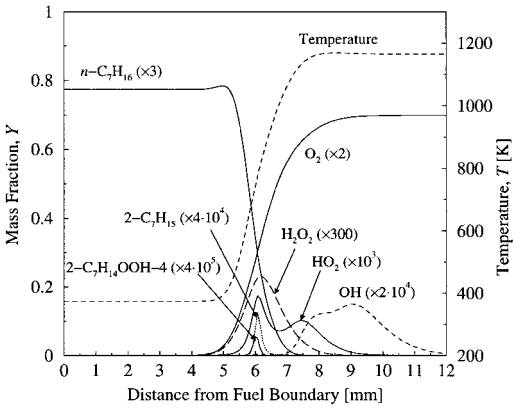

FIG. 7. Profiles of temperature, T, and mass fractions of C_7H_{16}, O_2, 2-C_7H_{14}OOH-5, 2-C_7H_{15}, OH, H_2O_2, and HO_2. These profiles are calculated using the short mechanism for $a_2 = 200$, $T_2 = 1164$ K, $Y_{F,1} = 0.387$, $T_1 = 378$ K, and $Y_{O_2,2} = 0.233$ (case A).

with O_2 that leads to the production of two OH radicals and chain-branching. This is the classical low-temperature branching sequence [10]. Fig. 6 shows the value of the sensitivity coefficient for the reaction 2-C_7H_{14}OOH-4 + O_2 = 2-C_7H_{14}OOH-4-O_2 in case A to be much larger than those in cases B and C. This result clearly shows that low-temperature chemistry is important at low strain rates. Fig. 6 shows that case C, which has the same value for T_2 as case A, does not exhibit low-temperature chemistry. Thus, strain has a greater influence than oxidizer temperature on low-temperature chemistry.

It is of importance to examine the influence of various reactions on the concentration of OH because it is the primary reactive radical produced by ignition reactions. It is also the primary radical that consumes the fuel and intermediate products under ignition conditions. Fig. 7 shows profiles of various species calculated using the short mechanism at a condition close to autoignition (case A). Here, distances are measured from the fuel boundary. The profile of HO_2 shows an interesting double peak.

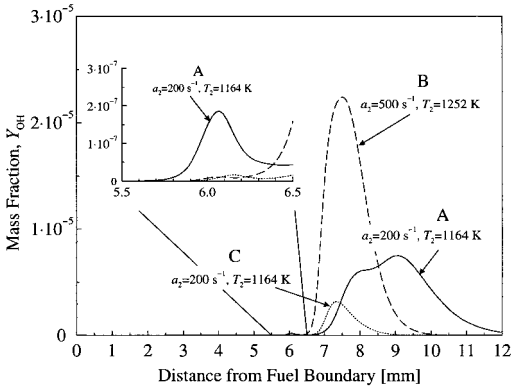

FIG. 8. Profiles of the mass fraction of OH, Y_{OH}, calculated using the short mechanism for $Y_{F,1} = 0.387$, $T_1 = 378$ K, and $Y_{O_2,2} = 0.233$.

The first peak is due to HO_2 production from low-temperature reaction paths given by R + $O_2 \rightarrow RO_2 \rightarrow QOOH \rightarrow$ alkene + HO_2. Here, Q represents C_nH_{2n} species or structures. The second HO_2 peak is due to high-temperature paths leading to HO_2 (e.g., HCO + $O_2 \rightarrow$ CO + HO_2). The profile of OH shows a small peak around 6 mm followed by a large peak around 9 mm with a "shoulder" around 8 mm. The shape of this profile is controlled by convection, diffusion, production, and consumption of OH. From a detailed reaction path analysis, the main reactions that consume OH are found to be

$$n\text{-}C_7H_{16} + OH = C_7H_{15} + H_2O \quad -45\%. \quad (R1)$$

$$CH_2O + OH = HCO + H_2O \quad -13\% \quad (R2)$$

$$HO_2 + OH = H_2O + O_2 \quad -7\% \quad (R3)$$

The main reactions that produce OH are

$$H + O_2 = OH + O \quad 17\% \quad (R4)$$

$$CH_3 + HO_2 = CH_3O + OH \quad 11\% \quad (R5)$$

$$H_2O_2 + M = OH + OH + M \quad 8\% \quad (R6)$$

$$C_7H_{14}OOH = C_7H_{14}O + OH \quad 14\% \quad (R7)$$

Here, the percentages refer to the contribution of the specified reaction to production of OH integrated across the flow field. Reaction R1 includes all reactions between n-C_7H_{16} and OH that give different isomers of C_7H_{15}, and reaction R7 includes all isomers of $C_7H_{14}OOH$ and $C_7H_{14}O$. The small peak in the profile of OH around 6 mm is due to production of this radical from low-temperature reactions (e.g., reaction R7 where a hydroperoxyheptyl radical produces a cyclic ether and an OH radical). This small peak occurs at 775 K, which as shown in Fig. 2, is in the negative temperature coefficient region (670–830 K) of a stoichiometric n-heptane/air mixture in a homogeneous reactor at a pressure of 1 bar. At increasing distance from the small peak of OH, the value of Y_{OH} begins to increase as the fuel is nearly consumed and intermediate species are formed. Prior to this point, the mass fraction of OH is small because it reacts with the fuel via reaction R1. Later, formaldehyde and other intermediate hydrocarbon species such as ethene and propene disappear, which leads to a further increase in the value of Y_{OH} for similar reasons. A number of reactions produce OH, which includes its production from decomposition of H_2O_2 via reaction R6. Reaction path analyses at different locations show that this reaction gives the "shoulder" in the profile of Y_{OH} around 8 mm. Reactions R4 and R5 make a significant contribution to the rates of production of OH around 7.5 mm, where the temperature and mass fractions of H, CH_3, and HO_2 are close to their peak values. Figure 7 shows a small increase of fuel around 5 mm caused by thermal diffusion. The increase in temperature from the fuel boundary enhances diffusion of nitrogen relative to the fuel.

Figure 8 shows profiles of Y_{OH} for the three cases considered here. With increasing strain rate, the small peak in the profile of OH disappears. This again indicates that strain has a greater influence than oxidizer temperature on low-temperature chemistry.

Concluding Remarks

The short chemical-kinetic mechanism for n-heptane was assembled from the detailed mechanism of Curran et al. [10] without introducing any empirical approximation. For non-premixed systems, this mechanism remains to be tested at pressures greater than 1 bar. It is still too large for application in computational fluid dynamic codes. To make such applications tractable, it will be useful to derive reduced chemical-kinetic mechanisms made up of global steps from this short mechanism.

Acknowledgments

The research at UCSD was supported by the U.S. Army Research Office through grant no. DAAD19-99-1-0259, under the direction of David M. Mann. Part of this work was performed under the auspices of the U.S. Department of Energy by the Lawrence Livermore National Laboratory under contract no. W-7405-ENG-48. The authors also acknowledge support of the German Science Foundation (DFG).

REFERENCES

1. Warnatz, J., *Proc. Combust. Inst.* 20:845–856 (1984).
2. Chevaliar, C., Louessard, P., Müller, U. C., and Warnatz, J., "A Detailed Low-Temperature Reaction

Mechanism of *n*-Heptane Auto-Ignition," in *Proceedings of the 2nd International Symposium on Diagnostics and Modelling of Combustion in Internal Engines*, S 93–97, The Japan Society of Mechanical Engineers, Tokyo, Japan, 1990.
3. Westbrook, C. K., Warnatz, J., and Pitz, W. J., *Proc. Combust. Inst.* 22:893–901 (1988).
4. Bui, M., and Seshadri, K., *Combust. Sci. Technol.* 79:293–310 (1991).
5. Lindstedt, R. P., and Maurice, L. Q., *Combust. Sci. Technol.* 107:317–353 (1995).
6. Ranzi, E., Gaffuri, P., Faravelli, T., and Dagaut, P., *Combust. Flame* 103:91–106 (1995).
7. Maurice, L. Q., "Detailed Chemical Kinetic Models for Aviation Fuels," Ph.D. thesis, University of London, 1996.
8. Bollig, M., Pitsch, H., Hewson, J. C., and Seshadri, K., *Proc. Combust. Inst.* 26:729–737 (1996).
9. Held, H. J., Marchese, A. J., and Dryer, F. L., *Combust. Sci. Technol.* 123:107–146 (1997).
10. Curran, H. J., Gaffuri, P., Pitz, W. J., and Westbrook, C. K., *Combust. Flame* 114:149–177 (1998).
11. Lindstedt, P., *Proc. Combust. Inst.* 27:269–285 (1998).
12. Seiser, R., Truett, L., Trees, D., and Seshadri, K., *Proc. Combust. Inst.* 27:649–657 (1998).
13. Seiser, R., Pitsch, H., Seshadri, K., Curran, H. J., and Pitz, W. J., "Experimental and Numerical Studies of Extinction and Autoignition of *n*-Heptane," Western States Section Fall Meeting of the Combustion Institute, University of California at Irvine, Irvine, California, October 25–26, 1999.
14. Seiser, R., Seshadri, K., Piskernik, E., and Liñán, A., *Combust. Flame*, 122:239–349 (2000).
15. Ciezki, H. K., and Adomeit, G., *Combust. Flame* 122:239–349 (2000).
16. Minetti, R., Carlier, M., Ribaucour, M., Therssen, E., and Sochet, L. R., *Combust. Flame* 102:298–309 (1995).
17. Griffiths, J. F., Halford-Maw, P. A., and Rose, D. J., *Combust. Flame* 95:291–306 (1993).
18. Griffiths, J. F., Halford-Maw, P. A., and Mohamed, C., *Combust. Flame* 111:327–337 (1997).
19. Seshadri, K., and Williams, F. A., *Int. J. Heat Mass Transfer* 21(2):251–253 (1978).
20. Peters, N., *Prog. Energy Combust. Sci.* 10:319–339 (1984).
21. Peters, N. and Rogg, B. (eds.), *Reduced Kinetic Mechanisms for Applications in Combustion Systems, Vol. m15 of Lecture Notes in Physics*, Springer-Verlag, Heidelberg, 1993, pp. 1–13.
22. Pitsch, H., "Entwicklung eines Programmpaketes zur Berechnung eindimensionaler Flammen am Beispiel einer Gegenstromdiffusionsflamme," Master's thesis, RWTH Aachen, Germany, 1993.
23. Curran, H. J., Gaffuri, P., Pitz, W. J., and Westbrook, C. K., unpublished results, 2000.
24. Lay, T., and Bozzelli, J. W., *J. Phys. Chem. A* 101:9505–9510 (1997).
25. Knyazev, V. D., and Slagle, I. R., *J. Phys. Chem. A* 102:1770–1778 (1998).
26. Seiser, R., Pitsch, H., Seshadri, K., Pitz, W. J., and Curran, H. J., *Intermediate and Short Mechanism for n-Heptane*, http://www-cms.llnl.gov/combustion/combustion_home.html.

COMMENTS

John Griffiths, University of Leeds, UK. Are you able to account for the diminishing importance of the low-temperature reactions as the strain rate is increased?

Author's Reply. We are able to account for the diminishing importance of low-temperature chemistry as the strain is increased. In our analysis, the influence of a given elementary reaction on the value of YOH is presumed to be a measure of its influence on critical conditions of autoignition. Fig. 6 shows that at a fixed oxidizer temperature of 1164 K, the values of sensitivity coefficients for reactions that characterize low-temperature chemistry are higher at the lower strain rate. This clearly shows the diminishing importance of low-temperature chemistry as the strain is increased.

•

Harsha Chelliah, University of Virginia, USA. You showed excellent agreement between experiments and modeling for extinction conditions, but comparisons were poor for counterflow ignition. Is it because of the quasi-steady ignition model used?

Author's Reply. consider the agreement between experimental measurements of oxidizer temperature at autoignition as a function of the strain rate and results of numerical calculation to be good. Close to critical conditions of autoignition, in the experiments the oxidizer temperature was increased by 1 K. At each temperature, steady conditions were maintained for approximately one minute. The temperature was increased until autoignition. It is therefore appropriate to use the quasi-steady ignition model in the computations.

•

Philippe Dagaut, CNRS/LCSR Orléans, France. Why is the cool flame more pronounced in the model than in the experiments (ignition of *n*-heptane versus $1/T$ in homogeneous conditions) at 3.2 and 13 bar and not at 40 atm? Is it due to the thermochemistry or the kinetics of the data obtained in this regime?

Author's Reply. We do not consider the relatively minor differences between simulated and experimental ignition delays to be important. These simulations were performed

with the assumption of homogeneous mixtures and no heat loss. Spatial variations in temperature inside the experimental device and heat losses could affect the agreement between the model and experiment.

However, your comment raises a very important question: why does the negative temperature coefficient (NTC) behavior become less pronounced with increasing pressure? This effect is observed both in the experiments and in the simulation (Fig. 2). As pressure is increased, the $R + O_2 \leftrightarrow RO_2$ equilibrium is shifted toward formation of RO_2. At higher pressures, the temperature must be raised higher than at lower pressures to dissociate RO_2, a process which shuts down the low-temperature chemistry and marks the start of the NTC region. Thus, the temperature at the start of the NTC region increases with pressure (Fig. 2). However, the end of the NTC region is caused by the influence of the dissociation of H_2O_2: $H_2O_2 + M = OH + OH + M$. The reactive OH radicals produced enhance the autoignition process. This reaction is pressure dependent, so that the rate of dissociation increases, with pressure becoming significant at lower temperatures when the pressure is raised. Thus, at higher pressures, dissociation of H_2O_2 terminates the NTC region before the NTC behavior can become as pronounced as that seen at lower pressures (Fig. 2).

•

Hai Wang, University of Delaware, USA. Based on your study and a series of previous work on the ignition of C_1–C_4 fuels in the counterflow configuration, it is quite conclusive that ignition is caused by high-temperature chain-branching chemistry under most conditions. What remains uncertain is the role of heat release at the ignition turning point. Have you looked into the coupled effects of chain branching and heat release on ignition strain rate?

Author's Reply. Numerical computations carried out in our study include the coupled effects of chain branching and heat release. We have not compared their relative influence.

•

Frederick Dryer, Princeton University, USA. You have chosen this configuration to emphasize the effect of diffusion on autoignition. It appears that while chemistry and thermochemistry sensitivities or results are considered, one might expect sensitivities to the assumption of particular diffusion coefficients used in the model. Indeed, the whole point is that some sensitivities may approach those of chemistry or thermochemistry. Have you investigated these sensitivities? Also, is the major diffusive sensitivity only thermal diffusion?

Author's Reply. We have not carried out detailed investigations of the sensitivities of molecular diffusivities of various species and thermal diffusivity on critical conditions of extinction and autoignition. As pointed out, these sensitivities may be comparable to those of key elementary reactions. The present study emphasizes the influence of flow field and chemistry on extinction and autoignition. Even if molecular diffusion is found to play a key role in autoignition and extinction, it is unlikely to change the key findings in this paper.

•

Chung K. Law, Princeton University, USA. We are pleased with your finding that high-temperature chemistry controls the ignition of strained diffusive systems. It agrees with the suggestion from our previous study on the counterflow ignition of ethane, propane, and butane at pressures below 5 atm [1] that "ignition . . . is initiated by fuel oxidation following the high-temperature mechanism of radical chain branching and with little contribution by low-to-intermediate temperature chemistry."

REFERENCE

1. Fotache, C. G., Kreutz, T. G., and Law, C. K., *Combust. Flame* 117:777–794 (1999).

Author's Reply. We agree with Prof. Law's observation.